Photoinduced Fluorescence Enhancement in CdSe/ZnS Quantum Dot Submonolayers Sandwiched between Insulating Layers: Influence of Dot Proximity

Junichi Kimura, Takafumi Uematsu, Shinya Maenosono,* and Yukio Yamaguchi

Department of Chemical System Engineering, University of Tokyo, Hongo 7-3-1, Bunkyo-ku, Tokyo 113-8656, Japan

Received: April 12, 2004; In Final Form: June 28, 2004

We report on photoinduced fluorescence enhancement (PFE) in a thin film of CdSe/ZnS core/shell quantum dots (QDs) sandwiched between a glass substrate and a silicon oxide layer and the dependence on the degree of proximity between the QDs. CdSe/ZnS QDs capped with tri-*n*-octylphosphine oxide (TOPO) were colloid-chemically synthesized, and the QD thin films of various thicknesses were then fabricated on glass substrates using a spin-coating technique. A SiO_x protective layer was subsequently sputtered on the QD thin film to prevent photoadsorption of water molecules and photooxidation. The fluorescence intensity monotonically increased under continuous excitation except for the case of the thinnest sample which exhibited intensity decay. Interestingly, the increasing rate of fluorescence intensity increases as a function of the number of QD layers, θ, to the extent of $\theta \leq 3.2$ and then decreases at $\theta \geq 3.2$. Fluorescence lifetime measurements indicate that the band-edge radiative relaxation probability becomes relatively higher as the fluorescence intensity is enhanced. Considering the experimental results with respect to QD submonolayers ($\theta \leq 1$), and in accordance with the theoretical model, PFE is elucidated by the charging effect of trapped electrons.

1. Introduction

Colloidal semiconductor quantum dots (QDs) have been the subject of much research because of their size-dependent photophysical properties and ability to adapt to novel applications, such as a biological label.[1,2] In particular, the optical and electric properties of II−VI semiconductor QDs, such as ZnS,[3−5] CdS,[6−8] and CdSe,[9−12] have been intensively studied. Recent advances in single-molecule and time-resolved spectroscopy and scanning probe microscopy have revealed that single QDs dispersed on/in a solid matrix exhibit fluorescence blinking,[12−15] spectral diffusion,[13−15] photoionization,[16,17] and many other single-dot properties. However, there is still much that is not understood about interdot interactions in a proximal state, though the interdot interactions in close-packed QD solids have been investigated to a certain extent, for example, Förster energy transfer[9,10] and broadening of the absorption spectrum.[18,19] Understanding interdot interactions in two- or three-dimensionally close-packed QD solids is essential not only because it is meaningful from a scientific viewpoint but also because QD solids are technologically important objects for applications such as an emissive layer for light emitting diodes,[20,21] a charge generation layer in photoelectric devices,[22] and a recording layer in optical storage media.[23,24]

Recently, reversible photoinduced fluorescence enhancement (PFE) phenomena in two-dimensionally close-packed QD layers[23−28] and in QD dispersions in various matrixes[29−32] have been reported. The chief characteristic of PFE is its reversibility, different from other irreversible fluorescence enhancement phenomena, such as photoannealing,[33] rapid photooxidation,[34] and oxygen adsorption.[35] PFE behavior is usually very complicated because it is influenced by many factors, such as the atmosphere, QD size, kinds of ligand molecules, kinds of substrates, and parameters of excitation light; thus, the mechanism has yet to be ascertained. For example, Xiao and coworkers have reported that PFE was observed in a vacuum and that the photoluminescence (PL) intensity responded in a species-specific manner when the QDs were exposed to different amine molecules.[29] When the QDs were exposed to triethylamine and irradiated continuously, the PL intensity increased. On the other hand, the PL intensity decreased when the QDs were exposed to benzylamine.[29] They attributed the PFE under vacuum to the reoptimization of ligand molecules. However, the mechanism of the species-specific responses has not been clarified yet.

Nevertheless, the following hypothetical mechanisms have been proposed to elucidate PFE: (1) photoadsorption of gaseous molecules (H_2O, etc.) on QD surfaces and the resulting passivation of surface states (photoactivation),[25,26,29] (2) photoinduced surface transformation[30] and/or photoinduced rearrangement of ligand molecules on QD surfaces[29,31] (phototransformation), (3) photoneutralization of local charged centers inside and outside of QDs (photoneutralization),[32] and (4) photoionization of QDs and subsequent trap filling by ejected carriers that leads to suppression of the ionization probability of the remaining neutral QDs (photoelectrification).[23,36]

In this study, we report on PFE behavior in a submonolayer of CdSe/ZnS core/shell QDs sandwiched between a glass substrate and a SiO_x layer and the dependence on the degree of proximity between the QDs by using atomic force microscopy (AFM), optical spectroscopy, and fluorescence lifetime measurement to provide further insights into the mechanisms of PFE.

2. Experimental Section

2.1. Materials. Tri-*n*-octylphosphine oxide (TOPO), trioctylphosphine (TOP), and CdO of the highest quality available were purchased from Aldrich, selenium powder (Se, 99.99% pure) was purchased from Strem Chemicals, tri-*n*-butylphos-

* Corresponding author. E-mail: shinya@chemsys.t.u-tokyo.ac.jp.

10.1021/jp048406b CCC: $27.50
Published on Web 08/07/2004

phine (TBP, 98+% pure), from Kanto Kagaku, and diethyldithiocarbamic acid zinc salt ($Zn[S_2CNEt_2]_2$, 99+% pure), from Tokyo Kasei Kogyo. Chloroform (99+% pure) and 1-butanol (1-BuOH, 98+% pure) were purchased from Wako Pure Chemical Industries.

2.2. Synthesis of CdSe/ZnS QDs. CdSe cores were colloid-chemically synthesized in a hot TOPO matrix according to the method described in ref 37 using CdO and Se−TBP as precursors. The average diameter of the CdSe cores estimated from the absorption peak wavelength was ~4 nm. ZnS shells were subsequently grown on CdSe cores using $Zn[S_2CNEt_2]_2$ as a single-molecule precursor.[38,39] A 4.0-g portion of TOPO and 0.1 g of CdSe QDs were put into a flask and heated to 250 °C in an Ar atmosphere. The melted TOPO/QD mixture was agitated for several minutes in Ar. 4.0 g of $Zn[S_2CNEt_2]_2$/TOP solution (6.3 wt %) was then added dropwise into the mixture, after which the reaction temperature was maintained at 250 °C for 60 min and 6 mL of 1-BuOH was added into the flask. Monodisperse CdSe/ZnS core/shell QDs capped with TOPO molecules were separated from the matrix by antisolvent precipitation and decantation. The ZnS shell thickness was calculated to be about two monolayers, and the average diameter of the CdSe/ZnS QDs was estimated to be ~5.2 nm, by taking into account the bulk lattice parameter of ZnS.[40]

2.3. Fabrication of QD Thin Films Sandwiched between Insulating Layers. The CdSe/ZnS QDs were redispersed in chloroform to QD concentrations of 0.01−3.3 wt %, and then, the QD/chloroform dispersions of different concentrations were spin-coated on acid-washed microcover glasses (25 mmϕ, Fisher Scientific). The speed, acceleration, and time of rotation were 3000 rpm, 2000 rpm/s, and 60 s, respectively. The QD thin films obtained were dried in a vacuum chamber for 1 h to remove volatile components and subsequently stored in a desiccator for 24 h at room temperature, maintaining dry and dark conditions. After that, a 200-nm-thick SiO_x ($x = 1.67$) protective layer was sputtered on the QD thin films by radio frequency (rf) magnetron sputtering to prevent any influence from atmospheric gases, such as H_2O[25,26] and O_2.[41] The composition of the sputtered SiO_x layer was determined by X-ray photoelectron spectroscopy (XPS). Sputtering was performed under the following conditions: Ar gas pressure, 0.5 Pa; gas flow rate, 30 sccm; rf power, 200 W; deposition rate, 5 Å/s, and deposition time, 400 s.

2.4. UV−vis Spectroscopy and AFM Observation of the QD Thin Films. The absorption spectra and microscopic images of the QD films were obtained by a UV−vis spectrophotometer (U-4100, Hitachi) and an atomic force microscope (SPA 300HV, Seiko Instruments) before the sputtering of the SiO_x protective layer. The average thickness of the QD layer, θ, was defined as

$$\theta = \frac{\int_{340}^{500} A(\lambda)\, d\lambda}{\int_{340}^{500} A_1(\lambda)\, d\lambda} \quad (1)$$

where λ, A, and A_1 represent the wavelength, absorption intensity of the QD film, and absorption intensity of the QD monolayer, respectively. The QD monolayer was fabricated using a 0.1 wt % dispersion. Note that the formation of the QD monolayer was confirmed by AFM; that is, the thickness was equal to a single QD size including TOPO, and the substrate surface was fully covered by QDs. The area intensity of the absorption spectrum was expected to be linearly proportional to the QD film thickness within our experimental conditions.[27,42] Hence, θ represents the number of QD layers, and the θ values of the samples used in the experiments were within 0.032−19.

The average number of adjacent dots (average coordination number), N, was also determined from the AFM images to quantify the degree of proximity between the QDs. The number of adjacent dots, n, was counted on 150 randomly selected QDs. Then, N was calculated according to the equation

$$N = \frac{1}{N_f}\sum_{i=1}^{N_f} n_i \quad (2)$$

where n_i and $N_f \geq 150$ represent the number of adjacent dots, n, of the ith QD and the total number of QDs selected to count n, respectively. Adjacency judgment was carried out by checking the AFM images carefully using image processing software.

2.5. Fluorescence Intensity and Lifetime Measurements. Photoluminescence (PL) spectra and the evolution of the PL peak intensity were measured by a fluorescence spectrophotometer (SPEX Fluorolog-3, JY Horiba). For progressive measurements, the sample was continuously irradiated by monochromatic light of a 360-nm wavelength (power, 15.6 μW/cm^2) and the PL area intensity, I (580−640 nm), was periodically recorded. All measurements were carried out at room temperature under ambient conditions (relative humidity, 20−30%) unless otherwise stated. The rate of intensity change is defined as $\Delta I(t) = 100[I(t) - I_0]/I_0$, where t and I_0 denote the time elapsed since the start of irradiation and the PL intensity at $t = 0$, respectively.

The fluorescence lifetimes of the QD films were measured by a frequency-domain fluorescence lifetime measurement system (SPEX Fluorolog-3 Tau, JY Horiba). In general, two methods are commonly employed to measure the decay of fluorescence intensity: (1) the time-domain method (pulsed excitation) and (2) the frequency-domain method (modulated excitation). For the frequency-domain method, a continuous excitation source is attenuated in a cyclical manner. The excited sample then will emit with a time lag that appears as a demodulation and phase shift from the input signal. The lifetime of the fluorescence is calculated from both the modulation and the phase shift. One advantage of the frequency-domain method is the ease of attainment of a high signal-to-noise ratio when an emission of the sample is weak. For details of the method, see ref 43.

A logarithmic sequence of 10 different frequencies, from 0.5 to 200 MHz, was applied to a Pockels cell. The sample was excited at 360 nm, and the phase and modulation of the fluorescence emission were recorded at 450−700 nm, with the average taken of three to five measurements for each frequency. The integration time at each frequency was 10 s. Since the excitation power is below 10 nW/cm^2, fluorescence enhancement during lifetime measurement is negligible. 1,4-Bis(5-phenyl-2-oxazolyl)benzene (POPOP), whose lifetime is known to be 1.35 ns (its excitation and emission wavelengths are 360 and 417 nm),[44] was used as the reference for the lifetime measurements.

3. Results and Discussion

Figure 1 shows the absorption and PL spectra of the QD/chloroform dispersion (3.3 wt %) and the QD films ($\theta = 19$) with and without the SiO_x sputtered layer. The QDs have typical absorption and PL spectra, exhibiting absorption peak blue shift in comparison to the bulk crystal. In the case of the QD film, a slight red shift of the PL peak is also observed in comparison to the dispersion. This red shift is due to the dipole−dipole

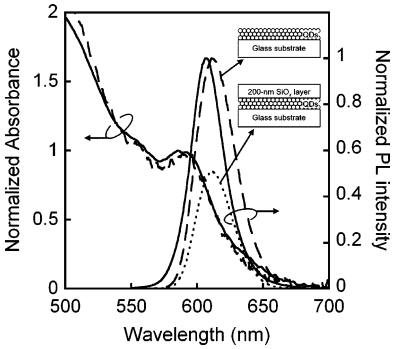

Figure 1. Absorption spectra of a QD/chloroform dispersion (3.3 wt %) (solid line) and a QD film ($\theta = 19$) (dashed line) and PL spectra of a dispersion (solid line), a film before SiO_x sputtering (dashed line), and a film after sputtering (dotted line). The absorption and PL spectra of a dispersion and a film before sputtering are normalized to each exciton peak and PL peak intensities, respectively. The PL spectrum of a film after sputtering is normalized to the PL peak intensity of a film before sputtering.

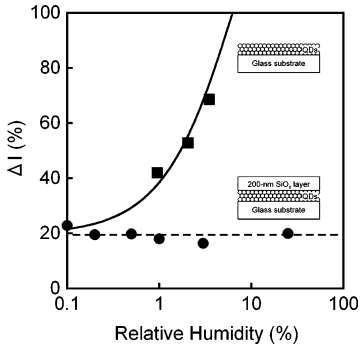

Figure 2. Rate of intensity change, $\Delta I = 100[I_{30} - I_0]/I_0$, plotted vs the relative humidity in QD monolayers ($\theta = 1$) with (circles) and without (squares) a SiO_x protective layer. The QD monolayers were continuously irradiated by 442-nm-wavelength light (power, 0.2 mW/cm^2) for 30 min at room temperature. The dashed and solid lines, respectively, represent the average rate of intensity change in the QD monolayer with a SiO_x layer, $\Delta\bar{I}_{SiO_x}$, and a single-exponential fit of the data of the bare QD monolayer, assuming that the PL intensity is proportional to the number of QDs photoactivated,[26] i.e., $\Delta I_{bare} = A(1 - e^{-k_a f}) + \Delta I^0_{bare}$, where A is a prefactor, k_a is a lumped rate constant, f is the relative humidity, and $\Delta I^0_{bare} \equiv \Delta\bar{I}_{SiO_x}$ is a value at $f = 0$.

interaction between the QDs in the close-packed film (Förster energy transfer).[9,10] The PL intensity significantly decreases after the SiO_x layer is sputtered, in comparison to that of the bare QD film. However, the shape of the PL spectrum remains unchanged, as shown in Figure 1. This PL quenching would be caused by degradation of the QD surfaces and/or an increase in the number of trap sites around the QDs during sputtering.

Figure 2 shows the humidity dependence of the rate of intensity change, ΔI, in QD monolayers ($\theta = 1$) with and without a SiO_x layer. The samples were continuously irradiated by 442-nm-wavelength excitation light (power, 0.2 mW/cm^2) for 30 min at room temperature, and then ΔI was calculated by $\Delta I = 100[I_{30} - I_0]/I_0$, where I_{30} represents the PL intensity after 30-min irradiation. The relative humidity was monitored by a hygrometer (accuracy, 0.1%) and controlled by introducing high-purity Ar gas into the measurement chamber of the spectrophotometer and changing the Ar flow rate. As shown in Figure 2, the ΔI value of the bare QD monolayer markedly increases as the relative humidity increases. ΔI monotonically increases up to 226% (relative humidity, 60%). The increase in ΔI as a function of humidity observed in the bare QD monolayer would be explained by the photoactivation mechanism.[25,26] On the other hand, the ΔI value of the QD monolayer with a SiO_x protective layer stays constant within the experimental humidity range, indicating that the SiO_x layer successfully prevents the photoactivation effect. Moreover, no blue shift of the PL peak was observed after the irradiation, indicating that the SiO_x layer also protects the QDs from photooxidation. The validity of the thickness of the SiO_x layer chosen in our experiments (200 nm) was verified by investigating ΔI with different thicknesses of the SiO_x layer. As a result, we found that ΔI decreases with an increasing thickness of the SiO_x layer and saturates when the thickness exceeds 100 nm. Hence, we concluded that a 200-nm-thick SiO_x layer is thick enough to block the gas diffusion.

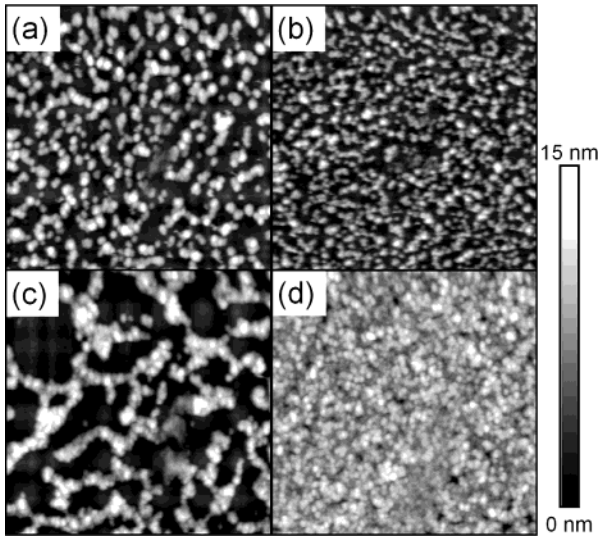

Figure 3. AFM images ($1 \times 1\ \mu m^2$) of QD submonolayers of different θ values obtained before sputtering: (a) $\theta = 0.032$; (b) $\theta = 0.12$; (c) $\theta = 0.27$; (d) $\theta = 1$.

Figure 3 shows the AFM images ($1 \times 1\ \mu m^2$) of the QD submonolayers ($\theta \leq 1$) obtained before sputtering of the SiO_x layer. The numbers of QD layers, θ values, of parts a, b, c, and d of Figure 3 are 0.032, 0.12, 0.27, and 1, respectively. The average numbers of adjacent dots, N values, of parts a, b, and c of Figure 3 are calculated to be 1.03 ± 0.95, 1.76 ± 0.99, and 3.56 ± 1.24, respectively. For the monolayer (Figure 3d), N is determined to be 6, assuming a hexagonal close-packed (hcp) structure. The microstructure of Figure 3c seems to differ qualitatively compared to those of Figure 3a and b. This might be due to the acceleration of QD aggregation in the QD/chloroform dispersion owing to a higher concentration of QDs.

Next, we show a plot of ΔI as a function of excitation time with respect to four different θ values in Figure 4a. The fluorescence intensity monotonically increases under continuous excitation except for the case of the sample with $\theta = 0.032$. Figure 4b shows a plot of $\Delta I = 100[I_{120} - I_0]/I_0$ as a function of θ, where I_{120} is the PL intensity after 120-min irradiation. ΔI increases with θ in the $\theta \leq 3.2$ region, while ΔI decreases when $\theta \geq 3.2$. The sample with $\theta = 0.032$ exhibits a negative ΔI value, as shown in Figure 4a and b. The monotonic decrease of ΔI in the $\theta \geq 3.2$ region suggests that QDs near the OD−glass and QD−SiO_x interfaces play important roles in PFE behavior. As shown in Figure 4c, N increases with θ, obviously indicating that ΔI is an increasing function with respect to N.

In addition, the PL intensities measured before SiO_x sputtering (I^*_0 values), just after sputtering (I_0), and after 120-min irradiation (with a SiO_x layer) (I_{120}) as a function of θ are shown in Figure 5. All PL intensity data are normalized to a value of I^*_0 at $\theta = 1$. As shown in Figure 5, I^*_0 linearly increases with θ in

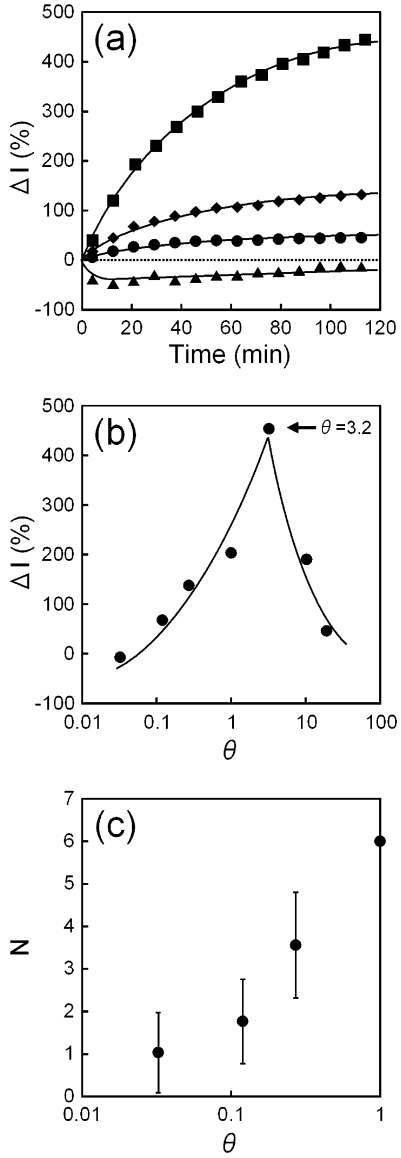

Figure 4. (a) Time variation of ΔI under continuous irradiation with respect to four different θ values. The triangles, diamonds, squares, and circles correspond to $\theta = 0.032$, 0.27, 3.2, and 19, respectively. The excitation source is a monochromatic light of a 360-nm wavelength (power, 15.6 μW/cm^2). Single logarithmic plots of (b) $\Delta I = 100[I_{120} - I_0]/I_0$ and (c) N as a function of θ are also shown. The solid lines in parts a and b are drawn as guides.

the double logarithmic plot, and its slope is determined to be 0.56. A value of the slope of I_0^* smaller than 1 suggests that the efficiency of energy transfer decreases with θ, because the probability of the existence of acceptor QDs within a critical energy-transfer distance decreases. On the other hand, the rate of PL quenching after the sputtering increases as θ decreases. This behavior would be due to an increase in the specific surface area of the QD ensemble and/or the resulting increase in the degree of degradation as θ decreases. If phototransformation[30,31] or photoneutralization[32] mechanisms operate, a QD film having a larger degree of surface degradation or a larger number of trap sites should exhibit a larger recovery rate. In other words, ΔI is expected to be a monotonically decreasing function of θ. However, as shown in Figure 4b, ΔI shows an opposite trend if $\theta \leq 3.2$. On the basis of the above discussions, it seems difficult to rationalize the PFE behavior observed in our experiments by phototransformation or photoneutralization mechanisms.

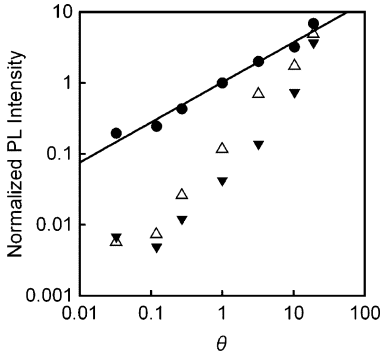

Figure 5. Double logarithmic plot of PL intensities measured before SiO_x sputtering (I_0^*) (filled circles), just after sputtering (I_0) (filled triangles), and after 120-min irradiation (with SiO_x) (I_{120}) (open triangles) as a function of θ. All PL intensity data are normalized to the value of I_0^* at $\theta = 1$. The solid line represents a linear fit of I_0^*, and its slope is 0.56.

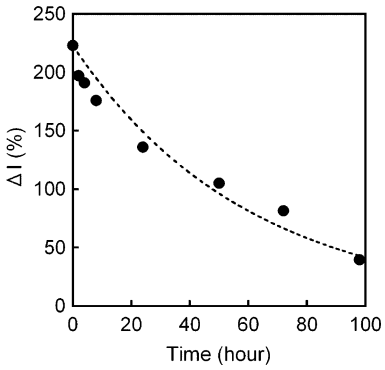

Figure 6. Typical decay behavior of the pre-enhanced PL intensity of a QD monolayer with a SiO_x layer under dark and ambient conditions. The dashed line represents a single-exponential fit of $I(t)/I(0) = e^{-t/\tau_d}$, where t is the time elapsed since the start of dark-decay measurement and $\tau_d \cong 60$ h is a time constant of decay.

According to the photoelectrification hypothesis,[23,36] these results would be capable of the following interpretation. That is, photoionization of a certain fraction of the QDs in the arrays leads to enhancement of the total emission efficiency as a result of a decrease in the ionization probability of the remaining neutral QDs. The photoionization of the QDs is thought to take place in any QD film, and the ionized QDs darken. An electron ejected from a darkened QD is trapped near the QD surface and suppresses further photoionization of adjacent QDs due to the electrostatic blockade effect. Because an exciton generated in the ionization-suppressed QD has a relatively higher probability of band-edge recombination, the emission efficiency of the ionization-suppressed QD is enhanced. This outweighs the darkening of a certain fraction of the QDs in the QD film and leads to enhancement of the total emission efficiency.[36] As estimated in ref 36, the electrostatic blockade effect is a short-range interaction; thus, a positive correlation between ΔI and N has been observed.

To confirm the reversibility of the observed PFE phenomenon, we measured the decay of the PL intensity enhanced beforehand. Figure 6 shows typical decay behavior of the PL intensity of a QD monolayer with a SiO_x layer under dark and ambient conditions. The PL intensity gradually attenuates with a time constant of 60 h that is determined by fitting a single-exponential function to the experimental data. Such a very slow relaxation might be due to long-lived electrons trapped near the OD−glass and QD−SiO_x interfaces. In fact, the time constant of neutralization of photoionized CdSe/CdS QDs on

silicon with a 2-nm oxide layer has been reported to be on the order of ~5 h.[17] If ≡SiO• defects exist in the SiO_x layer, they act as deep traps of electrons.[45] The energy gain of an electron capture on a ≡SiO• defect is around 3−4 eV.[45] These defects are possibly responsible for the slow PL decay shown in Figure 6. Hess and co-workers have reported that surface transformation in TOPO-capped CdSe QDs under a variety of circumstances results in PL quenching, but illumination of the QDs with above-band-gap light reverses the transformation (phototransformation).[30] The photorecovered PL intensity should be retained if the QDs are stored under dark and ambient conditions. However, the enhanced PL intensity returned to the intensity prior to irradiation.

The fluorescence decay kinetics of CdSe[46] and CdSe/ZnS[47,48] QDs have been intensively studied. Typically, the fluorescence lifetimes of QDs are determined by the time-domain method with pulsed excitation. The fluorescence decay curve is fitted by the following function

$$I(t_d)/I(0) = \sum_{j=1}^{N_r} a_j e^{-t_d/\tau_j} \quad (3)$$

where I and t_d denote the PL intensity and the time elapsed since the input of the excitation pulse, respectively. Here, a_j and τ_j are the contribution ratio and the lifetime of the jth component, respectively, and N_r normally corresponds to the number of relaxation pathways existing in the system. However, the fluorescence lifetime of a single CdSe/ZnS QD is known to be continuously distributed. For this reason, it is better to fit the decay curve to a stretched exponential function[47,48] given by

$$I(t_d)/I(0) = e^{-(t_d/\tau_{1/e})^{\beta}} \quad (4)$$

where $\tau_{1/e}$ and β are the 1/e lifetime and the exponent that represents the degree of lifetime distribution, respectively. Recently, Bawendi and co-workers measured fluorescence decay in the course of a blinking event by time-tagged, time-resolved (TTTR) measurements.[48] They found that the fluorescence decay at maximum intensity shows single-exponential behavior ($\beta \cong 1$) and that lifetimes are nearly constant from QD to QD and even from sample to sample. Thus, they speculated that the maximum-intensity lifetime is actually the radiative lifetime and that its value was ~25 ns. The emission efficiency fluctuations and divergence of the β value from 1, observed in their TTTR measurements, are thought to be due to variations of nonradiative relaxation pathways.

Both the average lifetime, $\langle\tau\rangle$, and the β value of the QD ensemble are expected to increase as the PL is enhanced according to the photoelectrification hypothesis, because photoionization-suppressed QDs lose the nonradiative relaxation (fast ionization−neutralization) pathway and have a relatively higher probability of band-edge recombination, as mentioned above. Thus, we investigated the temporal variation of fluorescence lifetime with irradiation time. Figure 7 shows phase and modulation spectra of the QD thin film with $\theta = 3.2$ measured before and after 120-min irradiation. Both the phase and modulation curves shift toward a lower frequency after irradiation, indicating that the florescence lifetime increases. To analyze the variation of fluorescence decay behavior in detail, we transformed the frequency-domain data measured after 0-, 20-, 60-, and 120-min irradiation to a time-domain stretched exponential function as follows. First, the phase and modulation spectra were fitted to eq 3 with $N_r = 4$ ($\chi^2 = 2-4.5$) using a

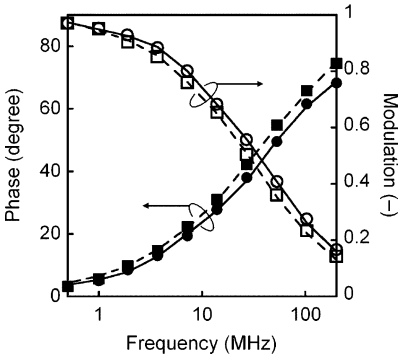

Figure 7. Phase (filled markers) and modulation (open markers) spectra of a QD thin film of $\theta = 3.2$ measured before (circles) and after (squares) 120-min irradiation. The solid and dashed lines represent the fitting results using eq 3 with $N_r = 4$ of experimental data before and after irradiation, respectively.

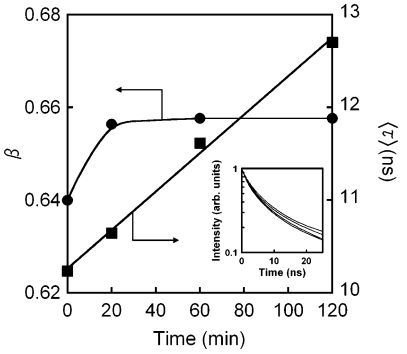

Figure 8. Average lifetime, $\langle\tau\rangle$, and exponent β of a QD thin film of $\theta = 3.2$ estimated by eqs 4 and 5 plotted vs irradiation time. The solid lines are drawn as guides. The inset shows time-domain decay curves generated by quadruple-exponential functions representing, starting from the bottom, measurement after 0-, 20-, 60-, and 120-min irradiation.

Globals Unlimited software package.[49] In Figure 7, the fitting results are shown by lines for comparison. Second, a time-domain decay curve was generated by a quadruple-exponential function obtained from the fitting. Finally, the generated curve was fitted to eq 4 by a least-squares method ($R \geq 0.996$). As a result, $\tau_{1/e}$ and β are specified for all cases. Average lifetime, $\langle\tau\rangle$, is given by

$$\langle\tau\rangle = \frac{\tau_{1/e}}{\beta}\Gamma\left(\frac{1}{\beta}\right) \quad (5)$$

where Γ represents the gamma function.[47] Figure 8 shows plots of $\langle\tau\rangle$ and β as functions of irradiation time. As expected, both $\langle\tau\rangle$ and β increase with irradiation time. The increase in β indicates that the unification of relaxation pathways proceeds. The increase in $\langle\tau\rangle$ indicates that the probability of nonradiative relaxation decreases. Consequently, these results suggest an increase in the band-edge relaxation probability with irradiation time.

Finally, we discuss the dependence of ΔI on the degree of proximity between QDs. As noted above, a positive correlation between ΔI and N is observed in the cases where $\theta \leq 1$ (see Figure 4c). According to the photoelectrification hypothesis, the normalized saturation PL intensity, I_∞/I_0, is given by[36]

$$\frac{I_\infty}{I_0} = \frac{\alpha - 1}{\alpha - \chi} \quad (6)$$

where α is the blocking factor that corresponds to the number of ionization-suppressed QDs including darkened QDs, $\chi = \alpha\gamma/$

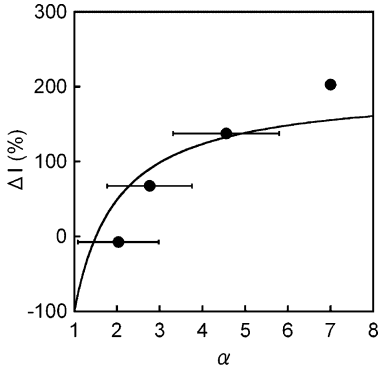

Figure 9. Dependence of ΔI on α. The circles and the solid line respectively represent experimental data and the theoretical fit according to eq 7 with $\zeta = 0.72$ and $\gamma = 3.4$.

$(1 + \zeta + \gamma)$, $\zeta = (k_r + k_n)/k_{exc}N_p$, and $\gamma = k_f^0/k_{exc}N_p$. Here, $k_{exc}N_p$ is the apparent rate constant of the generation of excited-state QDs. k_r and k_n are the rate constants of radiative (RR) and nonradiative (NR) relaxations. k_f^0 is the initial value of the rate constant of fast ionization (FI). For clarification, these processes are classified into internal (RR and NR) and interfacial (FI) relaxations. We examine the dependence of ΔI on N on the basis of eq 6. Since eq 6 is formulated with respect to a two-dimensional QD array,[36] the experimental data are confined to monolayer and submonolayer, i.e., $\theta \leq 1$, for the purpose of comparison.

Here, we assume $N + 1 \cong \alpha$, even though it is not exactly correct, because the electrostatic blockade effect has a directional characteristic and sensitively depends on the QD configuration.[36] Thus, α calculated as being equal to $N + 1$ is overestimated. However, for simplicity, we hereafter regard them as equivalent. The reason for adding 1 to N is that α includes the darkened QD. Assuming $I_{120} \cong I_\infty$, ΔI is written as

$$\Delta I = 100\left(\frac{I_\infty}{I_0} - 1\right) = 100\left(\frac{\chi - 1}{\alpha - \chi}\right) \tag{7}$$

By fitting eq 7 to the experimental data with ζ and γ as adjusting parameters, the tendency for the dependence of ΔI on α is found to be consistent with the experimental data, as shown in Figure 9. The values derived in the fitting are $\zeta = 0.72$ and $\gamma = 3.4$. The quantum efficiency, η, is given by

$$\eta = \frac{k_r}{k_r + k_n}\frac{\zeta}{\zeta + \gamma + \delta} \tag{8}$$

where δ is the dimensionless rate constant of trap filling by the ejected electrons and is estimated to be negligibly small in comparison to ζ and γ.[36] The value of η experimentally determined for the QD/chloroform dispersion is ~0.06; thus, the value of $k_r/(k_r + k_n)$ is calculated to be 0.34. This value is not that anomalous, supporting the hypothesis, although it appears relatively low.

4. Conclusion

Reversible photoinduced fluorescence enhancement (PFE) in a thin film of CdSe/ZnS core/shell QDs sandwiched between a glass substrate and a 200-nm SiO_x sputtered layer is described. The QD film was fabricated on a glass substrate via a spin-coating technique, and the degree of proximity between the QDs, which was defined as the average number of adjacent dots, N, was successfully tuned by changing the number of QD layers, θ. In the case of a QD submonolayer ($\theta \leq 1$), the rate of increase of the PL intensity was found to be an increasing function of N under continuous irradiation, suggesting that a proximity-dependent mechanism operates in the PFE phenomenon. In addition, the fluorescence lifetime of QD film was measured in the course of the PFE. Consequently, it was confirmed that both the average lifetime, $\langle\tau\rangle$, and the degree of lifetime distribution, β, of the QD ensemble increase as the PL is enhanced, indicating that a unification of the relaxation pathways to a band-edge relaxation proceeds with irradiation. Examining the dependence of the rate of the intensity enhancement, ΔI, on N and on the basis of the photoelectrification hypothesis, the proximity-dependent PFE behavior was construed as being the result of photoionization suppression of adjacent QDs due to the electrostatic blockade effect.

Acknowledgment. This work was supported by Grants-in-Aid for Scientific Research from the Ministry of Education, Culture, Sports, Science and Technology, Japan (MEXT), and from the "Nanotechnology Materials Program−Nanotechnology Particle Project" of the New Energy and Industrial Technology Development Organization (NEDO) based on funds provided by the Ministry of Economy, Trade and Industry, Japan (METI).

References and Notes

(1) Michalet, X.; Pinaud, F.; Lacoste, T. D.; Dahan, M.; Bruchez, M. P.; Alivisatos, A. P.; Weiss, S. *Single Mol.* **2001**, *2*, 261.
(2) Chan, W. C.; Maxwell, D. J.; Gao, X.; Bailey, R. E.; Han, M.; Nie, S. *Curr. Opin. Biotechnol.* **2002**, *13*, 40.
(3) Bhargava, R. N.; Gallagher, D.; Hong, X.; Nurmikko, A. *Phys. Rev. Lett.* **1994**, *72*, 416.
(4) Chen, W.; Wang, Z. G.; Lin, Z. J.; Lin, L. Y. *J. Appl. Phys.* **1997**, *82*, 3111.
(5) Zhu, Y.; Yuan, C. L.; Ong, P. P. *J. Appl. Phys.* **2002**, *92*, 6828.
(6) Chestnoy, N.; Harris, T. D.; Hull, R.; Brus, L. E. *J. Phys. Chem.* **1986**, *90*, 3393.
(7) Lakowicz, J. R.; Gryczynski, I.; Gryczynski, Z.; Murphy, C. J. *J. Phys. Chem. B* **1999**, *103*, 7613.
(8) Zhang, Y.; Wang, X.; Ma, M.; Fu, D. A.; Gu, N.; Lu, Z. H.; Xu, J.; Xu, L.; Chen, K. J. *J. Colloid Interface Sci.* **2003**, *266*, 377.
(9) Kagan, C. R.; Murray, C. B.; Bawendi, M. G. *Phys. Rev. B* **1996**, *54*, 8633.
(10) Murray, C. B.; Kagan, C. R.; Bawendi, M. G. *Annu. Rev. Mater. Sci.* **2000**, *30*, 545.
(11) Lifshitz, E.; Glozman, A.; Litvin, I. D.; Porteanu, H. *J. Phys. Chem. B* **2000**, *104*, 10449.
(12) Nirmal, M.; Dabbousi, B. O.; Bawendi, M. G.; Macklin, J. J.; Trautman, J. K.; Harris, T. D.; Brus, L. E. *Nature* **1996**, *383*, 802.
(13) Kuno, M.; Fromm, D. P.; Hamann, H. F.; Gallagher, A.; Nesbitt, D. J. *J. Chem. Phys.* **2000**, *112*, 3117.
(14) Neuhauser, R. G.; Shimizu, K. T.; Woo, W. K.; Empedocles, S. A.; Bawendi, M. G. *Phys. Rev. Lett.* **2000**, *85*, 3301.
(15) Kuno, M.; Fromm, D. P.; Hamann, H. F.; Gallagher, A.; Nesbitt, D. J. *J. Chem. Phys.* **2001**, *115*, 1028.
(16) Krauss, T. D.; O'Brien, S.; Brus, L. E. *J. Phys. Chem. B* **2001**, *105*, 1725.
(17) Cherniavskaya, O.; Chen, L.; Islam, M. A.; Brus, L. *Nano Lett.* **2003**, *3*, 497.
(18) Artemyev, M. V.; Bibik, A. I.; Gurinovich, L. I.; Gaponenko, S. V.; Jaschinski, H.; Woggon, U. *Phys. Status Solidi B* **2001**, *224*, 393.
(19) Kim, D. I.; Islam, M. A.; Avila, L.; Herman, I. P. *J. Phys. Chem. B* **2003**, *107*, 6318.
(20) Coe, S.; Woo, W. K.; Bawendi, M. G.; Bulovic, V. *Nature* **2002**, *420*, 800.
(21) Coe-Sullivan, S.; Woo, W. K.; Steckel, J. S.; Bawendi, M. G.; Bulovic, V. *Org. Electron.* **2003**, *4*, 123.
(22) Nozik, A. J. *Physica E* **2002**, *14*, 115.
(23) (a) Maenosono, S.; Dushkin, C. D.; Saita, S.; Yamaguchi, Y. *Jpn. J. Appl. Phys., Part 1* **2000**, *39*, 4006. (b) Maenosono, S.; Ozaki, E.; Yoshie, K.; Yamaguchi, Y. *Jpn. J. Appl. Phys., Part 2* **2001**, *40*, L638.
(24) Kimura, J.; Maenosono, S.; Yamaguchi, Y. *Nanotechnology* **2003**, *14*, 69.
(25) Cordero, S. R.; Carson, P. J.; Estabrook, R. A.; Strouse, G. F.; Buratto, S. K. *J. Phys. Chem. B* **2000**, *104*, 12137.

(26) Šimurda, M.; Němec, P.; Trojánek, F.; Mal×c6, P. *Thin Solid Films* **2004**, *453*−*454*, 300.
(27) Lowman, G. M.; Nelson, S. L.; Graves, S. M.; Strouse, G. F.; Buratto, S. K. *Langmuir* **2004**, *20*, 2057.
(28) Wang, Y.; Tang, Z. Y.; Correa-Duarte, M. A.; Liz-Marzán, L. M.; Kotov, N. A. *J. Am. Chem. Soc.* **2003**, *125*, 2830.
(29) Nazzal, A. Y.; Qu, L. H.; Peng, X. G.; Xiao, M. *Nano Lett.* **2003**, *3*, 819.
(30) Hess, B. C.; Okhrimenko, I. G.; Davis, R. C.; Stevens, B. C.; Schulzke, Q. A.; Wright, K. C.; Bass, C. D.; Evans, C. D.; Summers, S. L. *Phys. Rev. Lett.* **2001**, *86*, 3132.
(31) Jones, M.; Nedeljkovic, J.; Ellingson, R. J.; Nozik, A. J.; Rumbles, G. *J. Phys. Chem. B* **2003**, *107*, 11346.
(32) Oda, M.; Shen, M. Y.; Saito, M.; Goto, T. *J. Lumin.* **2000**, *87*−*89*, 469.
(33) Manna, L.; Scher, E. C.; Li, L. S.; Alivisatos, A. P. *J. Am. Chem. Soc.* **2002**, *124*, 7136.
(34) Wang, X. Y.; Zhang, J. Y.; Nazzal, A.; Xiao, M. *Appl. Phys. Lett.* **2003**, *83*, 162.
(35) Myung, N.; Bae, Y.; Bard, A. J. *Nano Lett.* **2003**, *3*, 747.
(36) Maenosono, S. *Chem. Phys. Lett.* **2003**, *376*, 666.
(37) Qu, L. H.; Peng, X. G. *J. Am. Chem. Soc.* **2002**, *124*, 2049.
(38) Motevalli, M.; O'Brien, P.; Walsh, J. R.; Watson, I. M. *Polyhedron* **1996**, *15*, 2801.
(39) Malik, M. A.; O'Brien, P.; Revaprasadu, N. *Chem. Mater.* **2002**, *14*, 2004.
(40) Dabbousi, B. O.; Rodriguez-Viejo, J.; Mikulec, F. V.; Heine, J. R.; Mattoussi, H.; Ober, R.; Jensen, K. F.; Bawendi, M. G. *J. Phys. Chem. B* **1997**, *101*, 9463.
(41) Koberling, F.; Mews, A.; Basche, T. *Adv. Mater.* **2001**, *13*, 672.
(42) Constantine, C. A.; Gattas-Asfura, K. M.; Mello, S. V.; Crespo, G.; Rastogi, V.; Cheng, T. C.; De Frank, J. J.; Leblanc, R. M. *J. Phys. Chem. B* **2003**, *107*, 13762.
(43) Lakowicz, J. R.; Maliwal, B. P. *Biophys. Chem.* **1985**, *21*, 61.
(44) Crowell, E.; Geng, L. *Appl. Spectrosc.* **2001**, *55*, 1709.
(45) Gritsenko, V. A.; Shaposhnikov, A. V.; Novikov, Yu. N.; Baraban, A. P.; Wong, H.; Zhidomirov, G. M.; Roger, M. *Microelectron. Reliab.* **2003**, *43*, 665.
(46) Underwood, D. F.; Kippeny, T.; Rosenthal, S. J. *J. Phys. Chem. B* **2001**, *105*, 436.
(47) Schlegel, G.; Bohnenberger, J.; Potapova, I.; Mews, A. *Phys. Rev. Lett.* **2002**, *88*, 137401.
(48) Fisher, B. R.; Eisler, H.-J.; Stott, N. E.; Bawendi, M. G. *J. Phys. Chem. B* **2004**, *108*, 143.
(49) Beechem, J. M.; Gratton, E.; Ameloot, M.; Knutson, J. R.; Brand, L. In *Topics in Fluorescence Spectroscopy*; Lakowicz, J. R., Ed.; Plenum Publishers: New York, 1991; Vol. 2, pp 241−305.